This article was downloaded by: [University of California, Berkeley]
On: 20 November 2014, At: 09:46
Publisher: Taylor & Francis
Informa Ltd Registered in England and Wales Registered Number: 1072954 Registered office: Mortimer House, 37-41 Mortimer Street, London W1T 3JH, UK

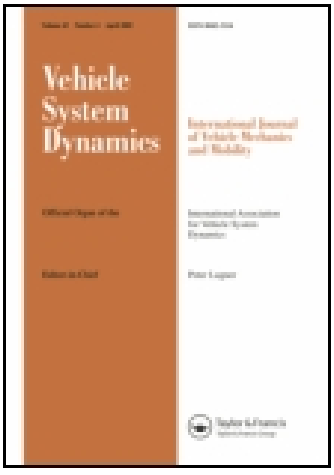

Vehicle System Dynamics: International Journal of Vehicle Mechanics and Mobility
Publication details, including instructions for authors and subscription information:
http://www.tandfonline.com/loi/nvsd20

Extended-Kalman-filter-based regenerative and friction blended braking control for electric vehicle equipped with axle motor considering damping and elastic properties of electric powertrain

Chen Lv[a], Junzhi Zhang[a] & Yutong Li[a]
[a] State Key Laboratory of Automotive Safety and Energy, Tsinghua University, Beijing 100084, People's Republic of China
Published online: 29 Oct 2014.

To cite this article: Chen Lv, Junzhi Zhang & Yutong Li (2014) Extended-Kalman-filter-based regenerative and friction blended braking control for electric vehicle equipped with axle motor considering damping and elastic properties of electric powertrain, Vehicle System Dynamics: International Journal of Vehicle Mechanics and Mobility, 52:11, 1372-1388, DOI: 10.1080/00423114.2014.938663

To link to this article: http://dx.doi.org/10.1080/00423114.2014.938663

PLEASE SCROLL DOWN FOR ARTICLE

Taylor & Francis makes every effort to ensure the accuracy of all the information (the "Content") contained in the publications on our platform. However, Taylor & Francis, our agents, and our licensors make no representations or warranties whatsoever as to the accuracy, completeness, or suitability for any purpose of the Content. Any opinions and views expressed in this publication are the opinions and views of the authors, and are not the views of or endorsed by Taylor & Francis. The accuracy of the Content should not be relied upon and should be independently verified with primary sources of information. Taylor and Francis shall not be liable for any losses, actions, claims, proceedings, demands, costs, expenses, damages, and other liabilities whatsoever or howsoever caused arising directly or indirectly in connection with, in relation to or arising out of the use of the Content.

This article may be used for research, teaching, and private study purposes. Any substantial or systematic reproduction, redistribution, reselling, loan, sub-licensing, systematic supply, or distribution in any form to anyone is expressly forbidden. Terms & Conditions of access and use can be found at http://www.tandfonline.com/page/terms-and-conditions

Downloaded by [University of California, Berkeley] at 09:46 20 November 2014

Vehicle System Dynamics, 2014
Vol. 52, No. 11, 1372–1388, http://dx.doi.org/10.1080/00423114.2014.938663

Downloaded by [University of California, Berkeley] at 09:46 20 November 2014

Extended-Kalman-filter-based regenerative and friction blended braking control for electric vehicle equipped with axle motor considering damping and elastic properties of electric powertrain

Chen Lv, Junzhi Zhang* and Yutong Li

State Key Laboratory of Automotive Safety and Energy, Tsinghua University, Beijing 100084, People's Republic of China

(*Received 15 January 2014; accepted 20 June 2014*)

Because of the damping and elastic properties of an electrified powertrain, the regenerative brake of an electric vehicle (EV) is very different from a conventional friction brake with respect to the system dynamics. The flexibility of an electric drivetrain would have a negative effect on the blended brake control performance. In this study, models of the powertrain system of an electric car equipped with an axle motor are developed. Based on these models, the transfer characteristics of the motor torque in the driveline and its effect on blended braking control performance are analysed. To further enhance a vehicle's brake performance and energy efficiency, blended braking control algorithms with compensation for the powertrain flexibility are proposed using an extended Kalman filter. These algorithms are simulated under normal deceleration braking. The results show that the brake performance and blended braking control accuracy of the vehicle are significantly enhanced by the newly proposed algorithms.

Keywords: electric powertrain dynamics; blended braking control; electric vehicles; extended Kalman filter; brake performance; regeneration efficiency

1. Introduction

The ever-heavier burden on the environment and dwindling energy resources require automobiles to be cleaner and more efficient. Studies show that in urban driving situations, about one-third to one half of the energy of the power plant is consumed during deceleration processes.[1–4] Among the key features of electrified vehicles, the regenerative braking system, which is capable of effectively improving the fuel economy by converting the vehicle's kinetic energy into electric energy during braking procedures, has become a hot topic of research and development among automakers, parts manufacturers, and researchers worldwide.[5–7]

Most manufactured electrified vehicles, including the Toyota Prius, Nissan Leaf, and Tesla Model S, are equipped with regenerative braking.[8–10] To guarantee the vehicle's brake performance, a mechanical brake is still needed. However, compared to the conventional friction brake, the regenerative brake presents quite different dynamic characteristics. For example, the motor's brake torque responds quickly and accurately, whereas a regenerative brake is

*Corresponding author. Email: jzhzhang@mail.tsinghua.edu.cn

© 2014 Taylor & Francis

Downloaded by [University of California, Berkeley] at 09:46 20 November 2014

significantly affected by the operation conditions of the motor and battery. In addition, its transmission path, via a gear box, driving shaft, and half-shaft to the wheel, is much longer than that of frictional brakes, which are just mounted on the side of a wheel. These features not only provide great potential for improving the vehicle dynamics performance under normal and critical driving conditions, but also present tremendous challenges to the existing brake theories and control methods. Therefore, researching the mechanism and control method for regenerative and friction brake blending is of great importance.

For cooperative control of regenerative braking and hydraulic braking, the existing research mainly focused on two aspects: braking energy management strategy and blended braking dynamic control.[11–13]

The task of braking energy management is to explore the potential of using regenerative braking to the maximum extent by reasonably allocating the regenerative braking force and friction braking force, improving an electric vehicle's energy efficiency as much as possible. These strategies are usually designed for a vehicle's kinetic energy regeneration during normal deceleration processes.[14–19]

However, blended braking coupling control targets dynamic processes. In contrast to a conventional internal combustion engine vehicle, an electrified vehicle equipped with a regenerative brake has three different braking states, i.e. friction braking, regenerative braking, and blended braking. These three braking states may occur independently or switch between each other frequently during one braking procedure. Particularly, because the dynamics of an electrified powertrain is quite different from that of the conventional friction brake, the introduction of the electric motor torque during deceleration may make it a new source of vibration and jerk on the system and vehicle levels. In addition, the dynamic modulation of the frictional braking force may also cause pressure fluctuations in the brake circuits, resulting in negative impacts on brake performance, brake comfort, and even the energy efficiency of the vehicle.[2] Thus, determining the electrified powertrain dynamics and its impact on blended brake control have become significant aspects of regenerative braking control. It is also important to determine how to dynamically couple the two different braking forces and coordinate the three different deceleration states to simultaneously ensure braking performance and improve the energy efficiency. In [20], a cooperative control algorithm for an electronic brake and regenerative braking for an automatic transmission-based hybrid electric vehicle was proposed to maintain the demanded braking force and driving comfort during a downshift with regenerative braking. In [21], a differential braking and driving vehicle stability control strategy was developed for a hybrid electric sport utility vehicle equipped with axle motors. In [7], several critical techniques that are suitable for the development and examination of HEVs with regenerative braking capability were proposed. In [22], a hybrid anti-lock braking system (ABS) solution for electric vehicles (EVs) and hybrid vehicles, endowed with in-wheel motors (IWMs) and friction brakes, was designed. However, the electrified powertrain dynamics and its impact on regenerative braking control performance are rarely seen in the existing research. Although some researchers have studied the powertrain system dynamics of EVs, they targeted the traction control under critical driving conditions or focused on the noise, vibration, harshness (NVH) performance of the vehicles.[23–25]

In this article, the blended braking control of an electric passenger car equipped with an axle motor is considered, along with the electric powertrain dynamics. The electric powertrain system, hydraulic brake, vehicle dynamics, and tyre are modelled. The electrified powertrain system dynamics and its impact on blended braking control are studied. To further enhance an electric vehicle's brake performance and energy efficiency, extended-Kalman-filter-based control algorithms for blended braking control are proposed. Simulations of the developed control algorithms during normal braking processes were carried out. Some of the simulation results are reported in this article.

Downloaded by [University of California, Berkeley] at 09:46 20 November 2014

2. System dynamics modelling

As shown in Figure 1, a regenerative braking system of an electrified passenger vehicle equipped with a central electric motor at the front axle is illustrated. The cooperative regenerative braking system, which comprises a hydraulic brake and an electric powertrain, the vehicle dynamics, and the tyre are modelled as follows.

2.1. *Electrified powertrain model*

The electric powertrain is built as a two-inertia model, as Figure 2 shows. In this simplified model, one inertia indicates the motor and the other one indicates the contribution from the load. A gearbox, representing the transmission, final drive, differential, and the inner constant-velocity joints, is located close to the motor inertia. The backlash contributions in the whole powertrain are lumped together into one single backlash. Assuming that the half-shafts have the same lengths, the values of left and right half-shaft torques are considered the same.

The motor drive unit adopted has a permanent-magnet synchronous topology. Regarding the effect of the electric system dynamics, the motor torque is modelled as a first-order reaction with a small time constant τ_{M} being taken into consideration, which can be expressed as follows:

$$\tau_{\mathrm{M}}\dot{T}_{\mathrm{M}} + T_{\mathrm{M}} = T_{\mathrm{M,ref}}, \tag{1}$$

where T_{M} is the actual value of motor torque and $T_{\mathrm{M,ref}}$ is the motor reference torque.

The equations for dynamics from the motor shaft to the gearbox output shaft are modelled by

$$J_{\mathrm{M}}^{*}\ddot{\theta}_{\mathrm{M}} = T_{\mathrm{M}} - T_{\mathrm{G}}, \tag{2}$$

where θ_{M} is the angular position of the motor, and the output torque of the gear box T_{G} and the equivalent moment of inertial J_{M}^{*} can be given by

$$T_{\mathrm{G}} = \frac{1}{\eta_1\eta_2\eta_{\mathrm{diff}}\eta_{\mathrm{j1}}(i_0 i_g)}\left(2T_{\mathrm{HS}} + \frac{1}{i_0 i_g}J_{\mathrm{HS}}\ddot{\theta}_{\mathrm{M}}\right), \tag{3}$$

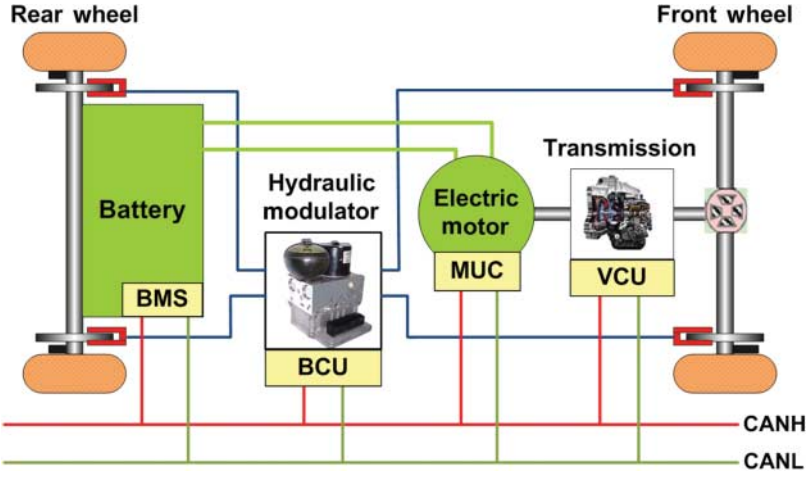

Figure 1. Scenario diagram of the cooperative regenerative braking system.

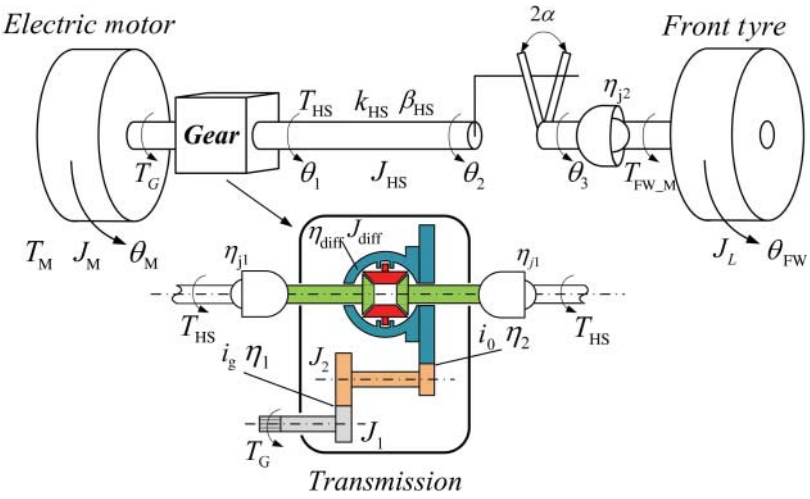

Figure 2. The simplified model of electric powertrain system.

$$J_{\mathrm{M}}^{*} = J_{\mathrm{M}} + J_1 + \frac{1}{\eta_1 i_g^2} J_2 + \frac{1}{\eta_1 \eta_2 (i_0 i_g)^2} J_{\mathrm{diff}}, \tag{4}$$

where η_1 and η_2 are the efficiencies of the first and the second stages of the transmission, respectively, η_{diff} is the efficiency of the differential, η_{j1} is the efficiency of the inner constant-velocity joint, J_{M} is the moment of inertia of the electric motor, J_1 is the moment of inertia of the gearbox input shaft, J_2 is the moment of inertia of the transmission shaft, J_{diff} is the moment of inertia of the differential, i_0 is final drive ratio, and i_g is the transmission ratio.

A flexible half-shaft with backlash is built connecting the gearbox and the load inertia. The nonlinear model of the half-shaft torque is given by [26]

$$T_{\mathrm{HS}} = k_{\mathrm{HS}}(\theta_{\mathrm{d}} - \theta_{\mathrm{b}}) + \beta_{\mathrm{HS}}(\dot{\theta}_{\mathrm{d}} - \dot{\theta}_{\mathrm{b}}), \tag{5}$$

where k_{HS} and β_{HS} are the stiffness and the damping coefficient of the half-shaft, $\theta_{\mathrm{d}} = \theta_1 - \theta_3 = \theta_{\mathrm{M}}/i_0 i_g - \theta_{\mathrm{FW}}$ is the total shaft displacement, and $\theta_{\mathrm{b}} = \theta_2 - \theta_3$ is the position in the backlash. θ_1,θ_2, and θ_3 are the angles at the indicated positions on the shaft.

The nonlinear model of backlash position is described as

$$\dot{\theta}_{\mathrm{b}} = \begin{cases} \max\left(0, \dot{\theta}_{\mathrm{d}} + \dfrac{k_{\mathrm{HS}}}{\beta_{\mathrm{HS}}}(\theta_{\mathrm{d}} - \theta_{\mathrm{b}})\right), & \theta_{\mathrm{b}} = -\alpha \\ \dot{\theta}_{\mathrm{d}} + \dfrac{k_{\mathrm{HS}}}{\beta_{\mathrm{HS}}}(\theta_{\mathrm{d}} - \theta_{\mathrm{b}}), & |\theta_{\mathrm{b}}| < \alpha \\ \min\left(0, \dot{\theta}_{\mathrm{d}} + \frac{k_{\mathrm{HS}}}{\beta_{\mathrm{HS}}}(\theta_{\mathrm{d}} - \theta_{\mathrm{b}})\right), & \theta_{\mathrm{b}} = \alpha \end{cases}, \tag{6}$$

where 2α is the backlash gap size.

The torque transmitted from the half-shaft to the wheel via the outer constant-velocity joint can be calculated based on Equation (7):

$$T_{\mathrm{FW_M}} = \eta_{\mathrm{j2}}\left(T_{\mathrm{HS}} - \frac{J_{\mathrm{HS}}}{2}\ddot{\theta}_{\mathrm{FW}}\right), \tag{7}$$

where η_{j2} is the efficiency of the outer constant-velocity joint.

Downloaded by [University of California, Berkeley] at 09:46 20 November 2014

Downloaded by [University of California, Berkeley] at 09:46 20 November 2014

2.2. *Hydraulic braking system*

To simulate and analyse the brake blending performance, the hydraulic brake system models, including valve dynamics and wheel brake pressure, have been developed. The schematic diagram of the hydraulic brake system is shown in Figure 3.

2.2.1. *Valve dynamics*

During the brake pressure build-up process, the hydraulic fluid flows through the normally open inlet valve from the master cylinder to the wheel cylinder. Therefore, the inlet valve model is of great importance for the simulation of hydraulic brake pressure modulation. The detailed descriptions of valve structure and models have been reported in [27,28].

The schematic diagram of the inlet valve with a coordinate system is presented in the right plot of Figure 3. The axial dynamic equation for the position of valve core can be expressed as

$$m_{\mathrm{v}}\ddot{x}_{\mathrm{v}} = F_{\mathrm{e}} - F_{\mathrm{s}} - F_{\mathrm{h}} - F_B \tag{8}$$

where m_{v} is the mass of the valve core, x_{v} is the displacement of the valve core, F_{e} is the electromagnetic force, F_{s} is the spring force, F_{h} is the hydraulic force, and F_B is the viscous force.

The electromagnetic force, acting on the valve core, can be expressed by the following relation [27]:

$$F_{\mathrm{e}} = \frac{(IN)^2}{(2R_{\mathrm{g}}l)}, \tag{9}$$

where I is the coil current, N is the number of turns, l is the air gap length, and R_{g} is the magnetic reluctance of the air gap.

The spring force can be given by the following relation:

$$F_{\mathrm{s}} = k_{\mathrm{s}}(x_{\mathrm{v}} + x_0), \tag{10}$$

where k_{s} is the stiffness coefficient of the return spring and x_0 is the preload displacement of the spring.

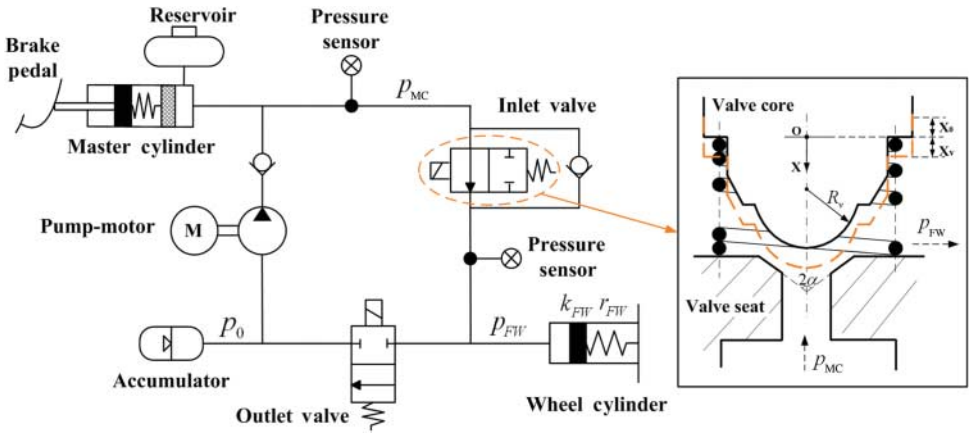

Figure 3. Schematic diagram of the hydraulic brake system.

Table 1. Key parameters of the electric powertrain and vehicle.

	Parameter	Value	Unit
Electric motor	Peak power	45	kW
	Maximum torque	144	Nm
Battery pack	Voltage	326	V
	Capacity	66	Ah
Vehicle	Total mass (m)	1360	kg
	Wheel base (L)	2.50	M
	Coefficient of air resistance (C_D)	0.32	—
	Nominal radius of tyre (r)	0.295	M
	Gear ratio	7.881	—

The viscous force is affected by the viscosity of the fluid and the movement velocity of the valve core, as shown in Equation (11):

$$F_B = B\dot{x}_v, \tag{11}$$

where B is the viscous damping coefficient.

The hydraulic force, exerted on the valve core by the fluid, can be calculated as [28]

$$F_h = \pi R_v^2(\cos\alpha)^2 \cdot \Delta p - 2\Delta p C_d^2 A_v \cos\alpha - \rho_{fluid} L\dot{q}_v, \tag{12}$$

$$A_v = \frac{\pi d_m}{R_v}\sqrt{R_v^2 - \frac{d_m^2}{4}} \cdot x_v, \tag{13}$$

where C_d is the flow coefficient of the inlet of the valve, ρ_{fluid} is the density of the hydraulic fluid, R_v is the spherical radius of the valve core, L is the damping length, q_v is the fluid flow of valve, Δp is the pressure difference across the valve, and d_m is the average diameter of the valve seat.

2.2.2. *Hydraulic brake pressure*

The structure of wheel cylinder is simplified to be a piston and a spring. Based on the valve dynamics analysed earlier in the paper, the wheel cylinder pressure can be represented as [28]

$$\dot{p}_{FW} = \frac{k_{FW}}{\pi^2 r_{FW}^4} C_d A_v \sqrt{\frac{2 \cdot \Delta p}{\rho_{fluid}}}, \tag{14}$$

where k_{FW} is the spring stiffness of the wheel cylinder and r_{FW} is the radius of the[!b] piston of the wheel cylinder.

2.3. *Vehicle dynamics and the tyre*

A model of vehicle dynamics with eight degrees of freedom has been built in MATLAB/Simulink by the present authors.[2,28] The tyre model, which is of great importance for research on braking, should be able to simulate the real tyre in both adhesion and sliding. In this article, the well-known Pacejka magic formula model is adopted.[29] The tyre behaviour can be accurately described under a combined longitudinal and lateral slip condition.

The detailed vehicle and tyre models developed were described in [2,28]. The feasibility and effectiveness of the models have been validated via hardware-in-the-loop tests and vehicle tests. Key parameters of the electrified powertrain and vehicle are listed in Table 1.

Downloaded by [University of California, Berkeley] at 09:46 20 November 2014

Downloaded by [University of California, Berkeley] at 09:46 20 November 2014

3. Electrified powertrain dynamics and its impact on performance of blended braking control

3.1. *Electric powertrain system dynamics*

The linearised model based on Equations (1)–(7) was implemented in a state-space formulation, as shown in Equation (15). The detailed formulation of the elements of the defined X and U vectors and A and B matrices is included in Appendix 1:

$$\begin{aligned} \dot{x} &= Ax + Bu, \\ y &= Cx + Du. \end{aligned} \tag{15}$$

Based on the linearised model, the system dynamics and properties are analysed in the following.

Figure 4(a) contains the Bode plots of the motor speed response to an input motor torque. The response of the motor speed is characterised by a sharp trough and peak pair at the anti-resonance frequency and resonance frequency of the system, respectively, showing the flexibility of the system.

The open-loop transfer function of the system with the wheel speed as the output can be given by

$$\frac{\omega_{\mathrm{FW}}}{T_{\mathrm{M}}} = \frac{\eta_{\mathrm{j2}}(\beta_{\mathrm{HS}}s + k_{\mathrm{HS}})}{i_g^* J_{\mathrm{M}}^* J_d s^3 + \left(i_g^* J_{\mathrm{M}}^* + \frac{2}{\eta^* i_g^*} \cdot J_d\right)\beta_{\mathrm{HS}} s^2 + \left(i_g^* J_{\mathrm{M}}^* + \frac{2}{\eta^* i_g^*} \cdot J_d\right) k_{\mathrm{HS}} s}, \tag{16}$$

where $i_g^* = i_0 i_g$, $\eta^* = \eta_1 \eta_2 \eta_{\mathrm{diff}} \eta_{\mathrm{j1}}$, and J_d is the moment of inertia of the load.

Figure 4(b) contains the Bode plots of the wheel speed to an input motor torque. In the low-frequency range, the driveline can be regarded as rigid. Once the frequency is greater than 30 rad/s, the response of the load speed is characterised by a resonance peak. When the damping coefficient decreases ($\beta_0 < \beta_1 < \beta_2 < \beta_3 < +\infty$), both the magnitude and phase responses are subject to amplitude growth at approximately the resonance point. Beyond 50 rad/s , with an increase in the frequency, the gradient of the magnitude response gradually deviates from –40 dB to –60 dB, which also demonstrates the flexibility of the powertrain system.

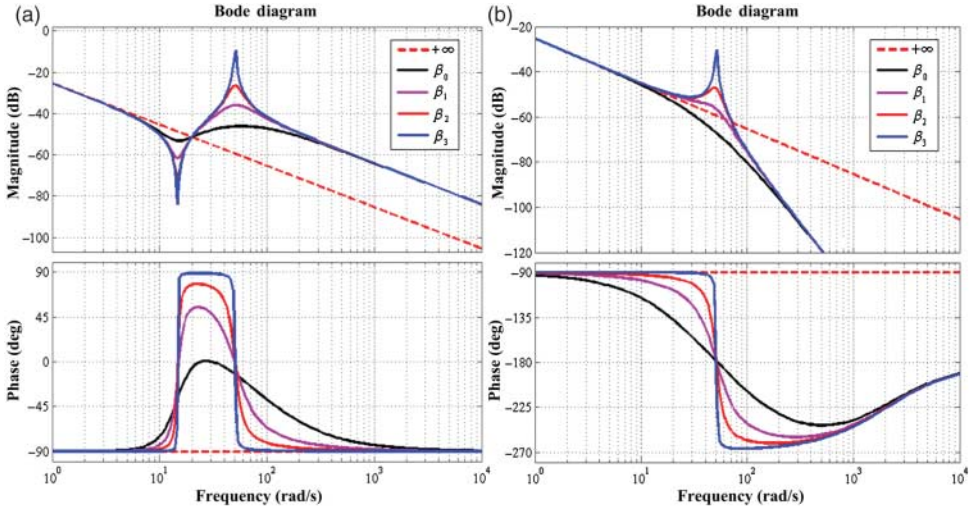

Figure 4. Bode plots of the motor and wheel speed responses to an input motor torque.

3.2. *Effect of powertrain dynamics on performance of blended braking control*

In existing studies on regenerative braking control, the transmitted motor torque on the wheel is usually equivalent to be an amplification of the motor's output regenerative torque via the gear ratio with transmission efficiencies.[13–15,20] A linearised block diagram of the conventional blended braking control is shown in Figure 5. The actual motor torque is used as a feedback signal for hydraulic brake modulation, whereas open-loop control is used for the electric motor torque.

However, based on the above discussion, the e-drivetrain, presenting a flexible property, cannot be regarded as a rigid system. Figure 6 shows the system response to step and sine-wave torque inputs in time domain. Both the values of the transmitted motor torque on the wheel under the two different inputs are smaller than the target with a small time delay.

Hence, simply considering the transmitted motor torque on the wheel as an amplified value based on the multiplying gear ratio of the motor output torque is not sufficient for an advanced brake blending control of electrified vehicles. And flexibility of the powertrain needs to be taken into consideration.

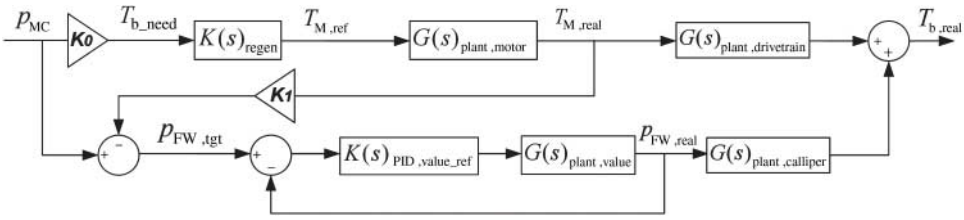

Figure 5. Block diagrams of the conventional blended braking control.

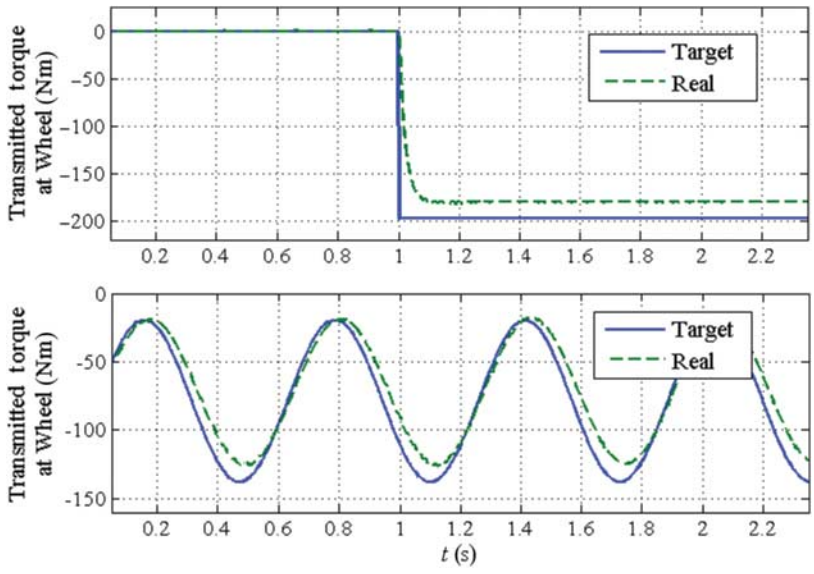

Figure 6. Powertrain responses to the step and sine-wave inputs in time domain.

Downloaded by [University of California, Berkeley] at 09:46 20 November 2014

Downloaded by [University of California, Berkeley] at 09:46 20 November 2014

4. Compensation control algorithm design

To further enhance the brake performance and improve the blending braking control effect for electric cars, compensation control that considers the impact of the electric powertrain dynamics needs to be developed.

4.1. *Transmitted torque observer design*

To compensate for the damping and elastic properties of the e-drivetrain, it is necessary to determine the value of the transmitted electric torque on the wheel.

Because the exact value of the transmitted torque on the wheel is difficult to directly measure on the plant, it is necessary to implement an extended Kalman filter to estimate it. The extended Kalman filter is based on the electrified powertrain model presented in the state-space formulation in Section 3. The mathematical formulation of the extended Kalman filter is illustrated as follows.

The process is governed by the nonlinear stochastic difference equation with a measurement Z, which can be given by Equations (17) and (18)[30]:

$$X_k = f\left(X_{k-1}, U_{k-1}, W_{k-1}\right), \tag{17}$$

$$Z_k = h\left(X_k, V_{k-1}\right), \tag{18}$$

where W is the process noise vector, h is the nonlinear measurement equation, and V is the measurement noise vector.

For the particular case studied in this work, the state vector at step k is

$$X_k = \left\{\dot{\theta}_{\mathrm{M}k}, \dot{\theta}_{\mathrm{FW}k}, \theta_{\mathrm{M}k}, \theta_{\mathrm{FW}k}, T_{\mathrm{M}k}\right\}^T. \tag{19}$$

The nonlinear system of difference equations $X_k = f\left(X_{k-1}, U_{k-1}, W_{k-1}\right)$ is shown as follows:

$$\begin{aligned}\dot{\theta}_{\mathrm{M}k} = &\left(1 - \frac{2\beta_{\mathrm{HS}}\Delta t_{KF}}{\eta^* i_g^{*2} J_{\mathrm{M}}^*}\right)\cdot\dot{\theta}_{\mathrm{M}k-1} + \frac{2\beta_{\mathrm{HS}}\Delta t_{KF}}{\eta^* i_g^* J_{\mathrm{M}}^*}\cdot\dot{\theta}_{\mathrm{FW}k-1} - \frac{2k_{\mathrm{HS}}\Delta t_{KF}}{\eta^* i_g^{*2} J_{\mathrm{M}}^*}\cdot\theta_{\mathrm{M}k-1}\\ &+ \frac{2k_{\mathrm{HS}}\Delta t_{KF}}{\eta^* i_g^* J_{\mathrm{M}}^*}\cdot\theta_{\mathrm{FW}k-1} - \frac{\Delta t_{KF}}{J_{\mathrm{M}}^*}\cdot T_{\mathrm{M}k-1} + w_{1k-1},\end{aligned} \tag{20}$$

$$\begin{aligned}\dot{\theta}_{\mathrm{FW}k} = &\frac{\eta_{\mathrm{j2}}\beta_{\mathrm{HS}}\Delta t_{KF}}{i_g^* J_{\mathrm{FW}}^*}\dot{\theta}_{\mathrm{M}k-1} + \left(1 - \frac{\eta_{\mathrm{j2}}\beta_{\mathrm{HS}}\Delta t_{KF}}{J_{\mathrm{FW}}^*}\right)\dot{\theta}_{\mathrm{FW}k-1} + \frac{\eta_{\mathrm{j2}}k_{\mathrm{HS}}\Delta t_{KF}}{i_g^* J_{\mathrm{FW}}^*}\theta_{\mathrm{M}k-1}\\ &- \frac{\eta_{\mathrm{j2}}k_{\mathrm{HS}}\Delta t_{KF}}{J_{\mathrm{FW}}^*}\theta_{\mathrm{FW}k-1} + \frac{\Delta t_{KF}}{J_{\mathrm{FW}}^*}T_{bx,\mathrm{FW},k-1} - \frac{T_{\mathrm{FW_H}}\Delta t_{KF}}{J_{\mathrm{FW}}^*} - \frac{f_0 F_{Z,\mathrm{FW}} R_W \Delta t_{KF}}{J_{\mathrm{FW}}^*} + w_{2k-1},\end{aligned} \tag{21}$$

$$\theta_{\mathrm{M}k} = \omega_{\mathrm{M}k-1}\Delta t_{KF} + \theta_{\mathrm{M}k-1} + w_{3k-1}, \tag{22}$$

$$\theta_{\mathrm{FW}k} = \omega_{\mathrm{FW}k-1}\Delta t_{KF} + \theta_{\mathrm{FW}k-1} + w_{4k-1}, \tag{23}$$

$$T_{\mathrm{M}k} = \left(1 - \frac{\Delta t_{KF}}{\tau_{\mathrm{M}}}\right)\cdot T_{\mathrm{M}k-1} + \frac{\Delta t_{KF}}{\tau_{\mathrm{M}}}\cdot T_{\mathrm{M,ref},k-1} + w_{5k-1}. \tag{24}$$

The measurement vector can be expressed as

$$Z_k = \{\tilde{\theta}_{\mathrm{M}k}, \tilde{\theta}_{\mathrm{FW}k}, \tilde{T}_{\mathrm{M}k}\}^{\mathrm{T}}. \tag{25}$$

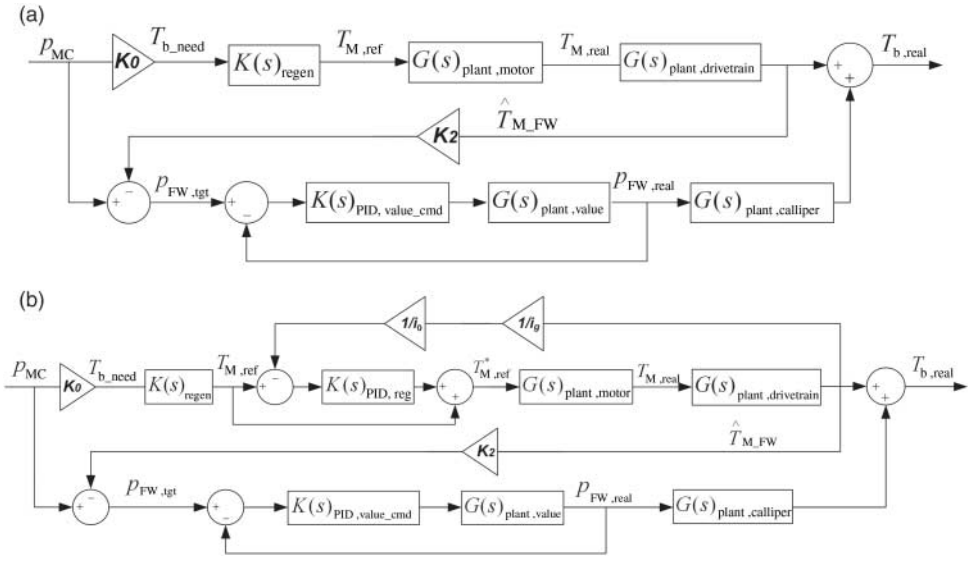

Figure 7. Block diagrams of the two developed compensation control algorithms.

The elements in the measurement vector at step k can be given by

$$\tilde{\theta}_{Mk} = \dot{\theta}_{Mk} + v_{1k}, \tag{26}$$

$$\tilde{\theta}_{FWk} = \dot{\theta}_{FWk} + v_{2k}, \tag{27}$$

$$\tilde{T}_{Mk} = T_{Mk} + v_{3k}. \tag{28}$$

The measured values of the angular speed of the motor and the front wheels and the measurement of the motor torque are provided by sensors. The noise level for the measurements is based on the experimental values reported in [31].

According to the general algorithm,[30] the extended Kalman filter is implemented in five steps, which are included in Appendix 2.

4.2. *Extended-Kalman-filter-based compensation control algorithm design*

Based on the extended Kalman filter designed, two compensation control algorithms for blended braking control are developed.

4.2.1. *Hydraulic-brake compensation control algorithm*

The idea of this strategy is to compensate the overall braking force by enhancing the friction brake. Figure 7(a) shows a block diagram of the hydraulic-brake compensation control algorithm. In this strategy, the transmitted motor torque on the wheel $\hat{T}_{M_FW}$, which is estimated by the extended Kalman filter designed earlier, is used as the feedback signal for hydraulic braking control. The target value for the hydraulic brake pressure is the difference between the master cylinder pressure and the equivalent brake pressure.

By compensating the hydraulic brake, the overall blended braking force at the front axle can be guaranteed to be equal to the required one. However, because the hydraulic braking force is increased, the regeneration efficiency will be decreased.

Downloaded by [University of California, Berkeley] at 09:46 20 November 2014

4.2.2. *Dual compensation control algorithm*

In order to improve the brake performance and regeneration efficiency simultaneously, the dual compensation control algorithm is designed, as shown in Figure 7(b). The aim of this strategy was to implement torque compensation by utilising the regenerative brake as much as possible. Based on the hydraulic-brake compensation control designed earlier, a tracking controller for motor torque is added in the inner loop, which outputs the compensated reference motor torque $T^*_{\mathrm{M,ref}}$. The compensated reference, which comprises a feed-forward reference torque and a compensation value of proportional-integral-derivative (PID) feedback controller, makes the motor torque control loop closed.

In this way, the overall braking force can be ensured, and the regeneration potential of the electric motor can be further explored, which improves the energy efficiency of the vehicle.

5. Simulation and analysis

5.1. *Simulation scenarios*

To evaluate the control performance of the designed algorithms during normal deceleration processes, simulations are carried out in MATLAB/Simulink with the models built in Section 2.

In simulations, the initial braking speed is set at 40 km/h. The master cylinder pressure is taken as a ramp input stabilising at 3 MPa. The road is assumed to be flat (no slope) and have a dry surface with a high adhesion coefficient of 0.8.

5.2. *Simulation and analysis*

5.2.1. *Simulation of baseline control algorithm*

The existing regenerative braking control algorithm presented in Section 3 is taken as a baseline. The simulation results of this strategy are shown in Figure 8.

During the deceleration, with the applying of regenerative brake, the front-wheel hydraulic pressure without compensation is gradually decreased to 0.30 MPa. Because of the flexibility of the drivetrain, the real transmitted motor torque on the wheel is much smaller than the expected one, which leads to the real blended torque being lower than the target value by nearly 40 N M. Moreover, at the end of the deceleration process (4.3–5 s), the control effect of the uncompensated coordination between the regenerative and the hydraulic brakes also deteriorates, which produces an unexpected jerk in the vehicle.

5.2.2. *Simulation of hydraulic-brake compensation algorithm*

Figure 9 shows the simulation results of the hydraulic-brake compensation control. In this improved algorithm, the front-wheel hydraulic pressure is under compensation control based on the feedback signal of the transmitted motor torque on the wheel estimated by the extended Kalman filter. Therefore, the front-wheel hydraulic pressure is modulated to 0.53 MPa, which is greater than that in the baseline strategy by 0.23 MPa. This compensates for the consumption of the motor torque loss in the driveline and guarantees that the blended braking torque on the wheel meets the total request. Furthermore, the jerk of the vehicle is also improved during the end of the braking process owing to the better coordination between the regenerative and hydraulic brakes.

Downloaded by [University of California, Berkeley] at 09:46 20 November 2014

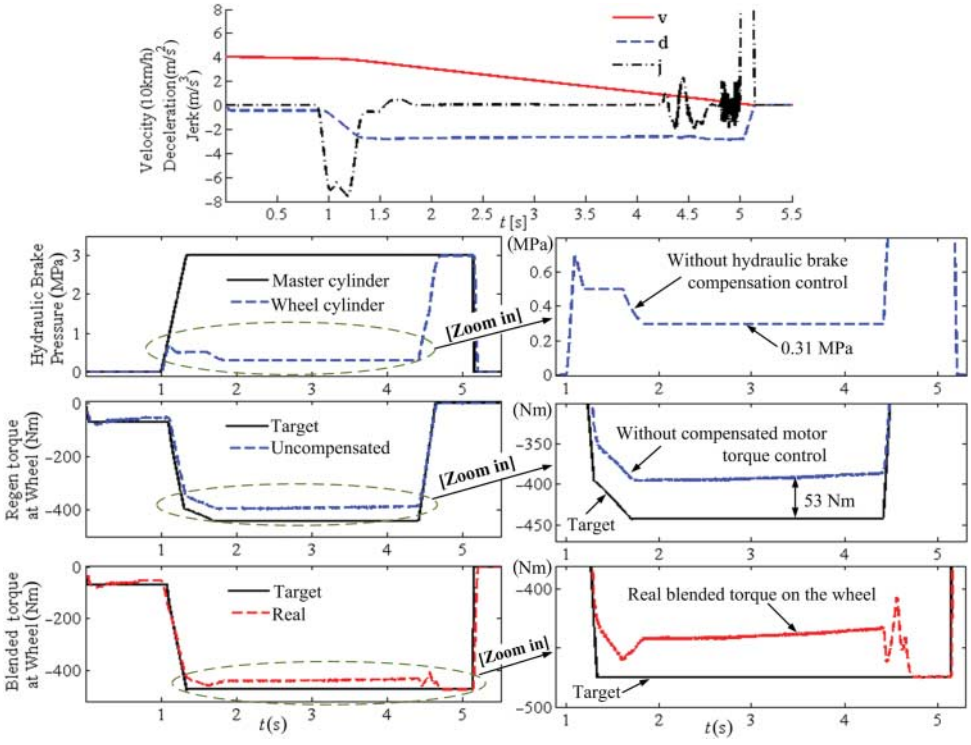

Figure 8. Simulation results of the baseline control strategy.

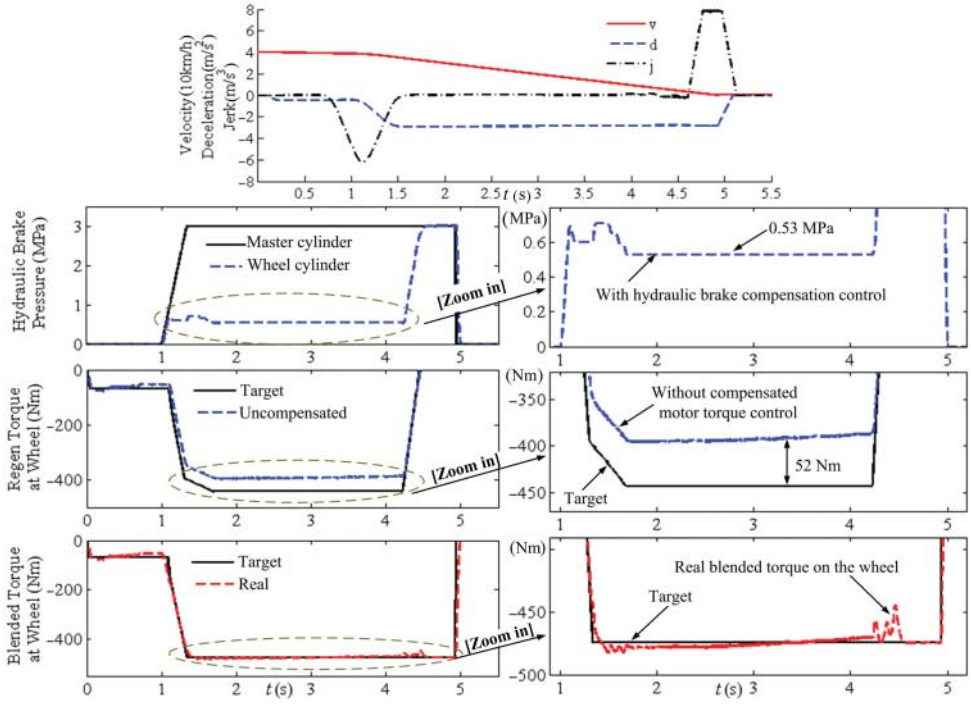

Figure 9. Simulation results of the hydraulic-brake compensation control strategy.

Downloaded by [University of California, Berkeley] at 09:46 20 November 2014

5.2.3. *Simulation of dual compensation algorithm*

Figure 10 shows the simulation results for the dual compensation control algorithm. Under compensated control, the real value of the transmitted motor torque on the front wheel meets the target value of 443 N M. Meanwhile, the hydraulic brake pressure is also compensated controlled based on the master cylinder pressure and the transmitted motor torque on the wheel, decreasing to as low as 0.27 MPa. As a result, the real blended torque on the front wheel remains consistent with a change in the target brake demand. The braking deceleration proceeds smoothly and jerk is significantly decreased, ensuring comfort and safety.

5.3. ***Comparisons of three control algorithms***

Regarding the results of the simulation mentioned previously, the coordination effects and the regeneration efficiencies of the three strategies are analysed as follows.

In order to evaluate the coordination effect of the three strategies, the root mean square error (RMSE) between the expected brake torque T_{target} and the real blended brake torque T_{blended} is selected as an evaluation parameter, as Equation (29) shows [28]:

$$\text{RMSE} = \sqrt{\frac{1}{n} \cdot \sum_{k=1}^{n} \left(T_{\text{target}}(k) - T_{\text{blended}}(k)\right)^2}. \tag{29}$$

The mean deceleration is adopted to evaluate the brake performance.

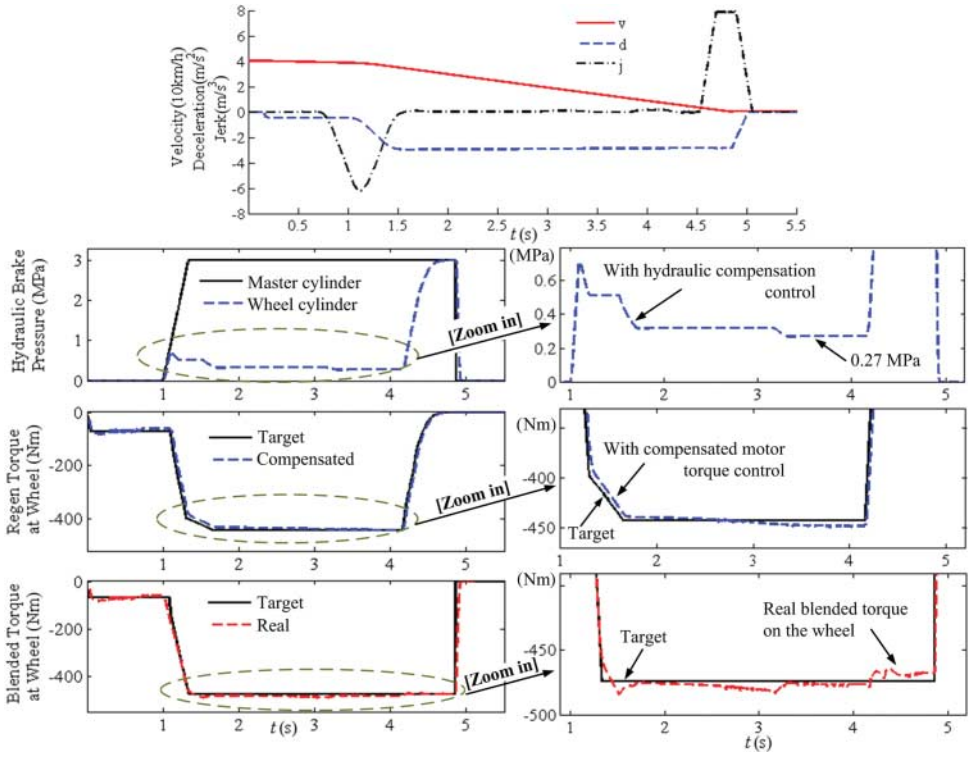

Figure 10. Simulation results of the dual compensation control strategy.

Downloaded by [University of California, Berkeley] at 09:46 20 November 2014

Table 2. Simulation results of brake performance and control accuracy.

Control algorithm	Mean deceleration (m/s^2)	Improvement of brake performance (%)	RMSE	Improvement of control accuracy (%)
Baseline	2.58	–	29.61	–
Hydraulic-brake compensation	2.72	5.43	10.05	66.06
Dual compensation	2.76	6.98	11.16	62.31

Table 3. Simulation results of regeneration efficiency.

Control algorithm	Recoverable energy (kJ)	Regenerated energy (kJ)	Regeneration efficiency (%)	Improvement (%)
Baseline	71.14	46.01	64.68	–
Hydraulic-brake compensation	71.36	43.38	60.79	– 6.01
Dual compensation	71.01	47.95	67.52	+ 4.39

To evaluate the regeneration capability of the control algorithms, the regeneration efficiency η_{regen} is used as an evaluation parameter [2]:

$$\begin{aligned}\eta_{\text{regen}} &= \frac{E_{\text{regen}}}{E_{\text{recoverable}}} \times 100\% \\ &= \frac{\int_{t0}^{t1} UI\mathrm{d}t}{\frac{1}{2}mu^2 - \int_{t0}^{t1} f_0 mgu\mathrm{d}t - \int_{t0}^{t1} \frac{C_D \cdot A}{21.15} \cdot (3.6u)^2 \cdot u\mathrm{d}t},\end{aligned} \tag{30}$$

where E_{regen} is the energy regenerated by an electric motor during regenerative braking and $E_{\text{recoverable}}$ is the maximum value of the recoverable energy. U is the output voltage of a battery pack, I is the charging current of the battery, u is the longitudinal speed of vehicle, f_0 is the rolling resistance coefficient of the tyre, C_D is the coefficient of air resistance, and A is the frontal area of the vehicle. t_0 is the initial braking time and t_1 is the final braking time.

Based on the simulation data, the RMSE, mean deceleration, and regeneration efficiency are listed in Tables 2 and 3. According to the data, the RMSE values of the two compensation strategies are 10.05 and 11.16, respectively, which are better than that of the baseline strategy at 29.61. This indicates an enhancement in the control accuracy of the blended brake torque of over 60%. Both the brake performances of the two compensation strategies are better than that of the baseline strategy. The dual compensation strategy has the highest regeneration efficiency (67.52%). However, it is followed by the baseline strategy at 64.68%, and then the hydraulic-brake compensation strategy at 60.79%, which verifies the analysis of the algorithms shown in Section 4.

6. Conclusion

This article discussed blended braking control for an electric passenger vehicle considering the flexibility of the electric powertrain. Models of the drivetrain and hydraulic brake system of an electric car equipped with an axle motor were built. Based on these models, the electric powertrain dynamics and its effect on the blended braking control performance were analysed. To further enhance the brake performance and energy efficiency of the vehicle, compensation control algorithms were proposed based on an extended Kalman filter. Simulations of the proposed algorithms were carried out under normal deceleration braking.

Downloaded by [University of California, Berkeley] at 09:46 20 November 2014

Simulation results showed that the brake performance and blended braking control accuracy of the case-study EV were significantly enhanced via using the newly proposed compensation algorithms by over 60%, compared to that of the baseline strategy. In addition, the dual compensation control also improved the regeneration efficiency by 4.39%, whereas the hydraulic-brake control strategy reduced this index by 6.01% due to the increased utilisation of the hydraulic brake in this algorithm.

Funding

This work was supported by the Natural Science Foundation of China [grant number 51075225].

References

[1] Gao Y, Ehsani M. Electronic braking system of EV and HEV – integration of regenerative braking, automatic braking force control and ABS. SAE Paper 2001-01-2478; The Society of Automotive Engineers (SAE), Warrendale, PA, USA; 2001.
[2] Zhang JZ, Lv C, Gou JF, Kong DC. Cooperative control of regenerative braking and hydraulic braking of an electrified passenger car. Proc Inst Mech Eng Part D J Automob Eng. 2012;226:1289–1302.
[3] Sovran G, Blaser D. Quantifying the potential impacts of regenerative braking on a vehicle's tractivefuel consumption for the US, European, and Japanese driving schedules. SAE Paper 2006-04-03; The Society of Automotive Engineers (SAE), Warrendale, PA, USA; 2006.
[4] Zhang J, Lv C, Qiu M, Li Y, Sun D. Braking energy regeneration control of a fuel cell hybrid electric bus. Energy Convers Manage. 2013;76:1117–1124.
[5] Kum D, Peng H,Bucknor NK. Supervisory control of parallel hybrid electric vehicles for fuel and emission reduction. J Dyn Syst Meas Control Trans ASME. 2011;133(6):061010-1-10. doi:10.1115/1.4002708
[6] Von Albrichsfeld C, Karner J. Brake system for hybrid and electric vehicles. SAE Paper 2009-01-1217; The Society of Automotive Engineers (SAE), Warrendale, PA, USA; 2009.
[7] Oleksowicz SA, Burnham KJ, Southgate A, Mccoy C, Waite G, Hardwick G, Harrington C, Mcmurran R. Regenerative braking strategies, vehicle safety and stability control systems: critical use-case proposals. Veh Syst Dyn. 2013;51:684–699.
[8] Nakamura E, Soga M, Sakai A, Otomo A, Kobayashi T. Development of electronically controlled brake system for hybrid vehicle. SAE Paper 2002-01-0300; The Society of Automotive Engineers (SAE), Warrendale, PA, USA; 2002.
[9] Ohtani Y, Innami T, Obata T, Yamaguchi T, Kimura T, Oshima T. Development of an electrically-driven intelligent brake unit. SAE Paper 2011-01-0572; The Society of Automotive Engineers (SAE), Warrendale, PA, USA; 2011.
[10] Fleming B. Electric vehicle collaboration-Toyota Motor Corporation and Tesla Motors. IEEE Veh Technol Mag. 2013;8:4–9.
[11] Crolla DA, Cao D. The impact of hybrid and electric powertrains on vehicle dynamics, control systems and energy regeneration. Veh Syst Dyn. 2012;50:95–109.
[12] Zhang JZ, Chen X, Zhang PJ. Integrated control of braking energy regeneration and pneumatic anti-lock braking. Proc Inst Mech Eng Part D J Automob Eng. 2010;224:587–610.
[13] Zhang J, Kong D, Chen L, Chen X. Optimization of control strategy for regenerative braking of an electrified bus equipped with an anti-lock braking system. Proc Inst Mech Eng Part D J Automob Eng. 2012;226:494–506.
[14] Ko J, Lee G, Ko S, Ahn S. Co-operative control of regenerative braking using a front electronic wedge brake and a rear electronic mechanical brake considering the road friction characteristic. SAE Paper 2012-01-1798; The Society of Automotive Engineers (SAE), Warrendale, PA, USA; 2012.
[15] Zhang J, Lv C, Yue X, Qiu M. Development of the electrically-controlled regenerative braking system for electrified passenger vehicle. SAE Paper 2013-01-1463; The Society of Automotive Engineers (SAE), Warrendale, PA, USA; 2013.
[16] Zhou Z, Mi C, Zhang G. Integrated control of electromechanical braking and regenerative braking in plug-in hybrid electric vehicles. Int J Veh Des. 2012;58:223–239.
[17] Bayar K, Biasini R, Onori S, Rizzoni G. Modelling and control of a brake system for an extended range electric vehicle equipped with axle motors. Int J Veh Des. 2012;58:399–426.
[18] Jeon K, Hwang H, Choi S, Hwang S, Choi SB, Yi K. Development of a fail-safe control strategy based on evaluation scenarios for an FCEV electronic brake system. Int J Automot Technol. 2012;13:1067–1075.
[19] Shu J, Zhang Y, Yin CL. Regenerative brake control using adaptive parameter estimation for a series-parallel hybrid electric bus. Int J Veh Des. 2010;54:35–46.
[20] Jo C, Ko J, Yeo H, Yeo T, Hwang S, Kim H. Cooperative regenerative braking control algorithm for an automatic-transmission-based hybrid electric vehicle during a downshift. Proc Inst Mech Eng Part D J Automob Eng. 2012;226:457–467.

Downloaded by [University of California, Berkeley] at 09:46 20 November 2014

[21] Bayar K, Wang J, Rizzoni G. Development of a vehicle stability control strategy for a hybrid electric vehicle equipped with axle motors. Proc Inst Mech Eng Part D J Automob Eng. 2012;226:795–814.
[22] De Castro R, Araujo RE, Tanelli M, Savaresi SM, Freitas D. Torque blending and wheel slip control in EVs with in-wheel motors. Veh Syst Dyn. 2012;50:71–94.
[23] Bottiglione F, Sorniotti A, Shead L. The effect of half-shaft torsion dynamics on the performance of a traction control system for electric vehicles. Proc Inst Mech Eng Part D J Automob Eng. 2012;226:1145–1159.
[24] Amann N, Bocker J, Prenner F. Active damping of drive train oscillations for an electrically driven vehicle. IEEE ASME Trans Mechatron. 2004;9:697–700.
[25] Yin D, Oh S, Hori Y. A novel traction control for EV based on maximum transmissible torque estimation. IEEE Trans Ind Electron. 2009;56:2086–2094.
[26] Nordin M, Galic' J, Gutman PO. New models for backlash and gear play. Int J Adapt Control Signal Process. 1997;11:49–63.
[27] Zhang J, Lv C, Yue X, Li Y, Yuan Y. Study on a linear relationship between limited pressure difference and coil current of on/off valve and its influential factors. ISA Trans. 2014;53:150–161.
[28] Lv C, Zhang J, Li Y, Sun D, Yuan Y. Hardware-in-the-loop simulation of pressure-difference-limiting modulation of the hydraulic brake for regenerative braking control of electric vehicles. Proc Inst Mech Eng Part D J Automob Eng. 2014;228:649–662.
[29] Pacejka HB, Bakker E. Magic formula tyre model. Veh Syst Dyn. 1993;21:1–18.
[30] Greg W, Gary B. An introduction to the Kalman filter. Chapel Hill, NC: Department of Computer Science, University of North Carolina at Chapel Hill; 2006.
[31] Hori Y, Toyoda Y, Tsuruoka Y. Traction control of electric vehicle: basic experimental results using the test EV "UOT Electric March". IEEE Trans Ind Appl. 1998;34:1131–1138.

Downloaded by [University of California, Berkeley] at 09:46 20 November 2014

Appendix 1

Each element of the matrices of the first equation of Equation (15) is illustrated here.

The state vector is

$$X = \begin{bmatrix} \dot{\theta}_{\mathrm{M}} & \dot{\theta}_{\mathrm{FW}} & \dot{\theta}_{\mathrm{V}} & \theta_{\mathrm{M}} & \theta_{\mathrm{FW}} & T_{\mathrm{M}} & T_{bx,\mathrm{FW}} \end{bmatrix}^{\mathrm{T}}.$$

The state matrix is

$$A = \begin{bmatrix} -\dfrac{2\beta_{\mathrm{HS}}}{\eta^* i_g^{*2} J_{\mathrm{M}}^*} & \dfrac{2\beta_{\mathrm{HS}}}{\eta^* i_g^* J_{\mathrm{M}}^*} & 0 & -\dfrac{2k_{\mathrm{HS}}}{\eta^* i_g^{*2} J_{\mathrm{M}}^*} & \dfrac{2k_{\mathrm{HS}}}{\eta^* i_g^* J_{\mathrm{M}}^*} & -\dfrac{1}{J_{\mathrm{M}}^*} & 0 \\ \dfrac{\eta_{\mathrm{j2}}\beta_{\mathrm{HS}}}{i_g^* J_{\mathrm{FW}}^*} & -\dfrac{\eta_{\mathrm{j2}}\beta_{\mathrm{HS}}}{J_{\mathrm{FW}}^*} & 0 & \dfrac{\eta_{\mathrm{j2}} k_{\mathrm{HS}}}{i_g^* J_{\mathrm{FW}}^*} & -\dfrac{\eta_{\mathrm{j2}} k_{\mathrm{HS}}}{J_{\mathrm{FW}}^*} & 0 & \dfrac{1}{J_{\mathrm{FW}}^*} \\ 0 & 0 & -\dfrac{\rho_{\mathrm{air}} C_D S R_W^3 \dot{\theta}_{\mathrm{V},0}}{J_{\mathrm{V}}^*} & 0 & 0 & 0 & -\dfrac{2}{J_{\mathrm{V}}^*} \\ 1 & 0 & 0 & 0 & 0 & 0 & 0 \\ 0 & 1 & 0 & 0 & 0 & 0 & 0 \\ 0 & 0 & 0 & 0 & 0 & -\dfrac{1}{\tau_{\mathrm{M}}} & 0 \\ 0 & 0 & 0 & 0 & 0 & 0 & -\dfrac{1}{\tau_W} \end{bmatrix}.$$

The input vector is

$$U = \begin{bmatrix} T_{\mathrm{M,ref}} & f_0 F_{Z,\mathrm{FW},0} R_W & f_0 F_{Z,\mathrm{RW},0} R_W & \dfrac{1}{2}\rho_{\mathrm{air}} C_D S R_w^3 \dot{\theta}_{\mathrm{V},0}^2 & T_{\mathrm{FW_H},0} & T_{\mathrm{RW_H},0} & \beta_W(\dot{\theta}_{\mathrm{V},0} - \dot{\theta}_{\mathrm{FW},0}) \end{bmatrix}^{\mathrm{T}}.$$

The input matrix is

$$B = \begin{bmatrix} 0 & 0 & 0 & 0 & 0 & 0 & 0 \\ 0 & -\frac{1}{J^*_{\mathrm{FW}}} & 0 & 0 & -\frac{1}{J^*_{\mathrm{FW}}} & 0 & 0 \\ 0 & 0 & -\frac{2}{J^*_{\mathrm{V}}} & \frac{1}{J^*_{\mathrm{V}}} & 0 & -\frac{2}{J^*_{\mathrm{V}}} & 0 \\ 0 & 0 & 0 & 0 & 0 & 0 & 0 \\ 0 & 0 & 0 & 0 & 0 & 0 & 0 \\ \frac{1}{\tau_{\mathrm{M}}} & 0 & 0 & 0 & 0 & 0 & 0 \\ 0 & 0 & 0 & 0 & 0 & 0 & \frac{1}{\tau_W} \end{bmatrix}.$$

Appendix 2

The detailed implementation of the extended Kalman filter is shown in the following steps.

Project the state ahead, which can be given by

$$\hat{X}_k^- = f\left(\hat{X}_{k-1}, U_{k-1}, 0\right).$$

Project the error covariance ahead, which is represented as

$$P_k^- = A_k P_{k-1} A_k^T + W_k Q_{k-1} W_k^T.$$

Compute the Kalman gain, as shown in the following:

$$K_k = \frac{P_k^- H_k^T}{H_k P_k^- H_k^T + V_k R_k V_k^T}.$$

Update estimate with measurement

$$\hat{X}_k = \hat{X}_k^- + K_k[Z_k - h(\hat{X}_k^-, 0)].$$

Update the error covariance:

$$P_k = (I - K_k H_k) P_k^-.$$

A is the Jacobian matrix of the derivatives of f with respect to x and is given by

$$A_{[i,j]} = \frac{\partial f_{[i]}}{\partial x_{[j]}}(\hat{x}_{k-1}, u_{k-1}, 0),$$

$$\begin{bmatrix} 1 - \frac{2\beta_{\mathrm{HS}}\Delta t_{KF}}{\eta^* i_g^{*2} J^*_{\mathrm{M}}} & \frac{2\beta_{\mathrm{HS}}\Delta t_{KF}}{\eta^* i_g^* J^*_{\mathrm{M}}} & -\frac{2k_{\mathrm{HS}}\Delta t_{KF}}{\eta^* i_g^{*2} J^*_{\mathrm{M}}} & \frac{2k_{\mathrm{HS}}\Delta t_{KF}}{\eta^* i_g^* J^*_{\mathrm{M}}} & -\frac{\Delta t_{KF}}{J^*_{\mathrm{M}}} \\ \frac{\eta_{\mathrm{j2}}\beta_{\mathrm{HS}}\Delta t_{\mathrm{KF}}}{i_g^* J^*_{\mathrm{FW}}} & 1 - \frac{\eta_{\mathrm{j2}}\beta_{\mathrm{HS}}\Delta t_{KF}}{J^*_{\mathrm{FW}}} + \frac{\partial T_{bx,\mathrm{FW}}}{\partial \dot{\theta}_W} \cdot \frac{\Delta t_{KF}}{J^*_{\mathrm{FW}}} & \frac{\eta_{\mathrm{j2}} k_{\mathrm{HS}}\Delta t_{KF}}{i_g^* J^*_{\mathrm{FW}}} & \frac{\eta_{\mathrm{j2}} k_{\mathrm{HS}}\Delta t_{KF}}{J^*_{\mathrm{FW}}} & 0 \\ \Delta t_{KF} & 0 & 1 & 0 & 0 \\ 0 & \Delta t_{KF} & 0 & 1 & 0 \\ 0 & 0 & 0 & 0 & 1 - \frac{\Delta t_{KF}}{\tau_{\mathrm{M}}} \end{bmatrix}.$$

Downloaded by [University of California, Berkeley] at 09:46 20 November 2014